









Cloud processing and weeklong ageing affect biomass burning aerosol properties over the south-eastern Atlantic

Haochi Che ^{1✉}, Michal Segal-Rozenhaimer ^{1,2,3✉}, Lu Zhang ¹, Caroline Dang^{3,4}, Paquita Zuidema ⁵, Amie Dobracki⁵, Arthur J. Sedlacek III ⁶, Hugh Coe ⁷, Huihui Wu⁷, Jonathan Taylor ⁷, Xiaoye Zhang⁸, Jens Redemann ⁹ & Jim Haywood^{10,11}

Southern Africa produces a third of global biomass burning emissions, which have a long atmospheric lifetime and influence regional radiation balance and climate. Here, we use air mass trajectories to link different aircraft observations to investigate the evolution of biomass-burning aerosols during their westward transport from Southern Africa over the south-eastern Atlantic, where a semi-permanent stratocumulus cloud deck is located. Our results show secondary organic aerosol formation during the initial 3 days of transport, followed by decreases in organic aerosol via photolysis before reaching equilibrium. Aerosol absorption wavelength dependency decreases with ageing, due to an increase in particle size and photochemical bleaching of brown carbon. Cloud processing, including aqueous-phase reaction and scavenging, contributes to the oxidation of organic aerosols, while it strongly reduces large diameter particles and single-scattering albedo of biomass burning aerosols. Together, these processes resulted in a marine boundary layer with fewer yet more oxidized and absorbing aerosols.

¹Department of Geophysics, Porter School of the Environmental and Earth Sciences, Tel Aviv University, Tel Aviv 6997801, Israel. ²Bay Area Environmental Research Institute, Moffett Field, CA 94035, USA. ³NASA Ames Research Center, Moffett Field, CA 94035, USA. ⁴Oak Ridge Associated Universities, Oak Ridge, TN 37831, USA. ⁵Rosenstiel School of Marine and Atmospheric Sciences, University of Miami, Miami, FL 33149, USA. ⁶Brookhaven National Laboratory, Upton, NY 11973, USA. ⁷Department of Earth and Environmental Sciences, University of Manchester, Manchester M13 9PY, UK. ⁸State Key Laboratory of Severe Weather (LASW) and Key Laboratory of Atmospheric Chemistry of CMA, Chinese Academy of Meteorological Sciences, Beijing 100081, China. ⁹School of Meteorology, University of Oklahoma, Norman, OK 73072, USA. ¹⁰College of Engineering, Mathematics and Physical Science, University of Exeter, Exeter EX4 4QF, UK. ¹¹Met Office Hadley Centre, Exeter EX1 3PB, UK. ✉email: haochiche@tauex.tau.ac.il; msegalro@tauex.tau.ac.il

Southern Africa contributes to roughly one-third of the global biomass burning (BB) emissions through widespread fires^{1,2}. These BB aerosols exhibit various physical and chemical properties depending on fuel source, combustion phase (i.e., flaming, smouldering, pyrolysis), and atmospheric ageing³. Despite extensive studies, the radiative forcing by BB aerosols in the south-eastern Atlantic (SEA) region remains uncertain^{4–9}.

The mass, composition, morphology, and size distribution of BB aerosols evolve with ageing^{10–14}, resulting in uncertainties in BB aerosol-radiation-cloud interactions. BB aerosols in the SEA have a long lifetime in the atmosphere, and as such suggesting ageing can have an important yet unclear effect on aerosol properties^{15,16}. Aerosol ageing can cause organic aerosol (OA) mass to either increase by functionalisation or oligomerisation reactions or decrease by fragmentation^{12,17,18}. Laboratory experiments show a considerable increase in the OA (70% on average) resulting from the formation of secondary organic aerosol (SOA)^{12,19–21}. While field observations have reported conflicting results^{10,22–24}, with the majority of field observations suggest negligible changes^{25–29}. Brown carbon (BrC), a particular type of OA, is of interest due to its ability to absorb radiation near-UV and visible wavelengths³⁰. Ageing can produce secondary BrC through multiphase reactions^{31–34}; it can also reduce BrC, known as “BrC bleaching”^{26,30,35}. Current climate models generally consider OA to be scattering only, leading to large uncertainties in some regions, where BrC contributes substantially or even dominates the total aerosol absorption^{30,36}.

The number size distribution of BB aerosol evolves with ageing due to collision and coalescence, as well as condensation of SOA on BB particles^{23,25}, affecting cloud condensation nuclei (CCN) concentration and, in turn, indirect radiative forcing. The evolution of the physical and chemical properties of BB aerosol can result in changes in its optical properties. Single-scattering albedo (SSA) and absorption Ångström exponent (AAE) are two critical parameters in calculating the aerosol direct radiative effects. Given that SSA of BB aerosols is a strong controlling factor for the sign and magnitude of direct radiative forcing in the SEA³⁷, and SSA depends on particle size, shape, and chemical composition, the aforementioned changes via ageing can therefore affect direct radiative forcing in the SEA by changing SSA.

Cloud processing, one particular type of ageing, is unique in providing a supersaturated environment and liquid droplets which facilitate aqueous-phase reactions³⁸. In addition, it can also modulate aerosol distribution by Brownian capture as well as collision and coalescence. The frequently observed smoke in the marine boundary layer in Ascension Island³⁹ highlights the importance of cloud processing in the SEA. However, as only few studies focus on cloud processing, its effect on aerosols remains uncertain⁴⁰. Therefore, cloud processing has been treated separately in this work for a comparative study of its impact.

The lack of understanding of ageing and cloud processing in the SEA also comes from the sparsity of observations. In previous studies, laboratory experiments have focused on examining aerosol ageing within a few hours while the African BB aerosol over the SEA undergoes several days of ageing^{15,16}. Most field observations have challenges in investigating the evolution of BB aerosols due to the spatial scales required to capture aging sufficiently. To address these issues, two synergistic aircraft measurement campaigns were performed in the SEA in 2017. By linking aircraft observations from different regions (different transport time of plumes) with air mass trajectories, we are able to investigate the evolution of BB aerosols in the specific airmass by using a Lagrangian methodology. Here we report on the evolution of BB aerosol in the SEA region and their chemical, optical, and physical properties.

Results and discussion

Oxidation and evolution of organic aerosols. As shown in Fig. 1(a, b), we find that cloud processing plays a vital role in affecting OA mass. For dry cases, where aerosols do not undergo cloud processing (grey dots), OA enhancement factors $\Delta(\text{OA}/\text{CO})$ are slightly above or around zero, indicating OA mass increases lightly or remains unchanged with ageing. Whereas for wet cases, where aerosols have been subjected to cloud processing (coloured dots), $\Delta(\text{OA}/\text{CO})$ values are negative, showing the decrease in OA mass. The reduced OA can be up to 70%, indicating a strong wet removal of BB particles by the clouds. The extent of wet removal may be related to the cloud liquid water content, as most of the wet cases (ageing time <100 h) show the higher cloud liquid water content, the greater reduction of OA mass. In addition to clouds, temperature is another important factor influencing OA matter and ageing. Figure 2(b) illustrates the temperature variations during the transport of the linked BB aerosols, where the temperature increases for those samples with clearly decreased OA mass. This result suggests that the increase in temperature may also contribute to reducing OA mass, likely resulting from the evaporation of high volatile OA. However, as the aerosol spends more time in the atmosphere, it subsides from the free troposphere and can reach altitudes with warmer temperatures, suggesting the reduction in OA and the increase in temperature may be independent. Dang et al. (2022)⁴¹ found that OA measured in ORACLES has lower volatility than CLARIFY OA; therefore, the change in OA mass due to temperature is likely to be minor, suggesting that cloud processing may be the dominant factor behind the reduction in OA mass.

Two of the dry cases clearly exhibit the increase of OA in Fig. 1(a, b), indicating the formation of SOA. Although the modified combustion efficiency (MCE) of those two cases are slightly lower than others, they are still higher than 0.98 (Supplementary Notes 3), suggesting all BB emissions in our study are from similar flaming fires, consistent with recent findings¹⁶. Statistical significance tests for MCE and $\Delta(\text{OA}/\text{CO})$ find that the two variables are not significantly correlated (p -value > 0.05), although the small sample size may contribute to large uncertainties. Therefore, the increased OA mass results from an ageing process rather than different burning conditions. As seen in Fig. 2(a), the two samples with increased $\Delta(\text{OA}/\text{CO})$ are accompanied by high upstream CO concentrations, while the samples with substantially unchanged $\Delta(\text{OA}/\text{CO})$ in the dry environment have low CO concentrations. Therefore, this may indicate that the increase in OA may be related to the high concentration of the plume still observed after ~40 h of initial ageing (at the upstream sampling locations, Supplementary Notes 2), as it may preserve high concentrations of volatile organic gases. From these two $\Delta(\text{OA}/\text{CO})$ increased samples, we find that $\Delta(\text{OA}/\text{CO})$ decreases with further ageing (ageing hours since the upstream observation), indicating that SOA formation peaks before ~30 h of further ageing, after which OA mass starts to decrease. The decrease of OA mass may indicate fragmentation processes such as photolysis, which can cause carbon-carbon bond cleavage and result in smaller and more volatile compounds, becoming dominant after ~30 h of further ageing. This finding is consistent with a filter-based study which found that CLARIFY has more volatile OA, whereas the OA in ORACLES generally is less volatile⁴¹. After ~60 h of further ageing, $\Delta(\text{OA}/\text{CO})$ remains around zero for dry cases, indicating that SOA formation and OA volatilisation rates are in equilibrium, resulting in a negligible change in OA mass, suggesting the remaining OA is more resistant to photolysis.

For both no-cloud and cloud-processed cases, the oxidised organic fraction of f_{44} increases with ageing in Fig. 1(c, d), despite OA mass decreasing or remaining unchanged (Fig. 1c, d). The

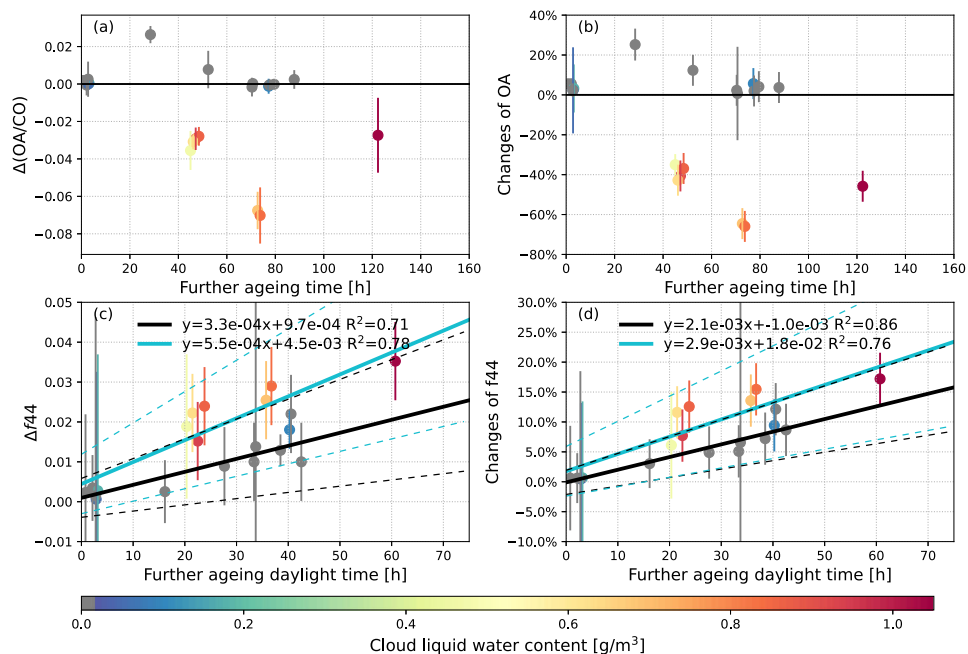


Fig. 1 Evolution of organic aerosol (OA) with ageing. **a** OA enhancement factor $\Delta(\text{OA}/\text{CO})$ and **b** changes of OA in percentage as ageing time increases since the upstream observation (further ageing time); **c** enhanced f_{44} and **d** changes of f_{44} in percentage with further ageing time for daylight hours only, during the transportation of the biomass burning aerosols between upstream and downstream observations. The dots are mean values for linked cases, and the error bars are standard errors calculated from Gaussian error propagation. The colourmap indicates the mean cloud liquid water content within the last day of transport as derived from the SEVIRI satellite data (as detailed in the method section), and the grey colour represents samples with no cloud processing. The black horizontal lines in **a**, **b** are the zero lines of OA mass changes. The dashed and solid lines in **c**, **d** are linear regressions and 95% confidence intervals for samples with cloud processing (cyan coloured lines) and without (black coloured lines). The fitted equations and R^2 values are shown in each of the plots.

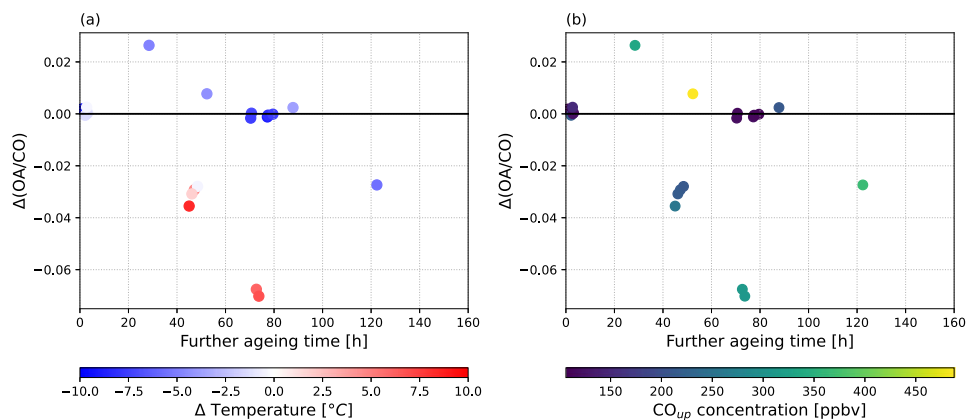


Fig. 2 Evolution of organic aerosol (OA) enhancement factor with ageing. **a** Coloured by variation in temperature and **b** by upstream CO concentrations (CO_{up}) during transport of the linked biomass burning aerosol samples. The further ageing time are ageing hours since the upstream observation.

increased amount of f_{44} is linearly correlated with the hours of daylight time, indicating that the oxidation of organic aerosol is generally dominated by photochemical or OH (also related to sunlight) induced reactions. Both no-cloud and cloud-processed samples have good linear relationships for f_{44} and daylight time, with R^2 higher than 0.7, and all samples are within the 95% confidence intervals. f_{44} has a higher rate of increase in cloud-processed cases rather than no-cloud cases at comparable ageing points, indicating the contribution of cloud processing to f_{44} . There are two potential ways in which cloud processing can result in a higher Δf_{44} , (1) increases the fraction of SOA via aqueous-phase reactions, and (2) reduction in the mass of less oxidised OA components. As the air mass enters the cloud layer, the mass of

both high and low oxidised OA is reduced by the cloud droplets and supersaturated water vapour. However, when the air mass exits the clouds, it may carry aerosols which formed from the evaporation of cloud droplets. The OA of those cloud residual particles is highly hygroscopic and has a high oxidized fraction due to the aqueous phase oxidation they have been subject to ref. 42,43, resulting in an overall increased f_{44} in the observed particles. As well, OA in BB aerosols that are not removed by cloud droplets may also undergo heterogeneous reactions, forming SOA with high f_{44} . This finding highlights the importance of cloud processing, as it increases the highly oxidised OA mass, resulting in more easily activated CCN and further affecting the stratocumulus cloud deck when BB aerosol interacts

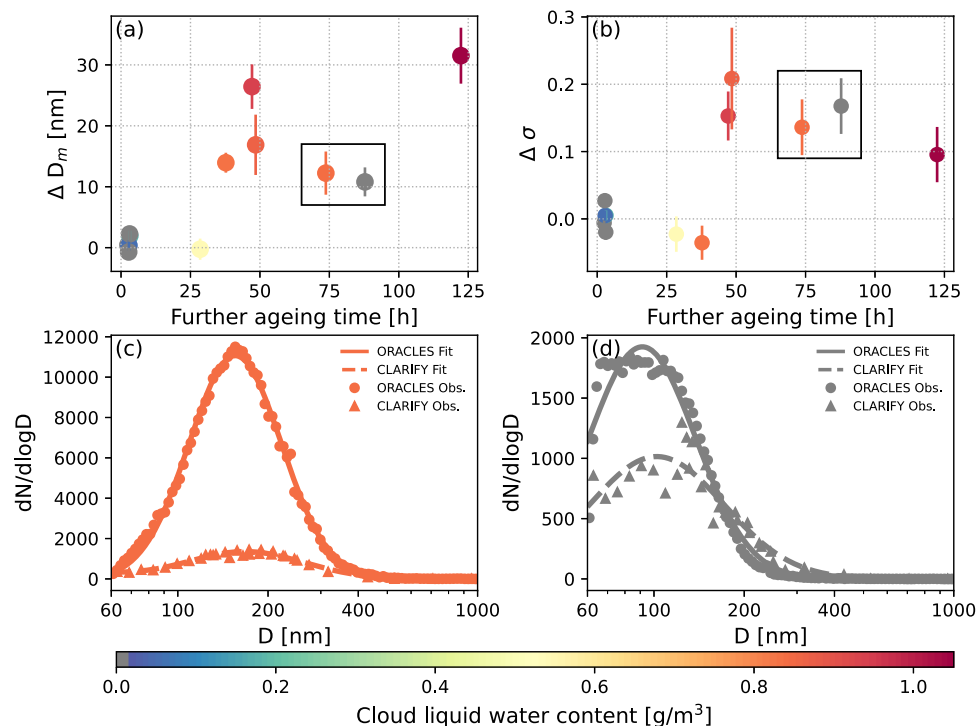


Fig. 3 Evolution of aerosol size distribution with ageing. **a** Aerosol mode diameter D_m and **b** geometric standard deviation σ with further ageing time. **c, d** Corresponding aerosol size distributions from two cases in the black box of **a** and **b**. The dots and error bars in **a, b** are mean values and standard errors from Gaussian error propagation. The dots in **c, d** are mean particle size distribution measured by upwind ORACLES (ObseRVations of Aerosols above CLouds and their intERactionS) campaign, whereas the triangles are means from downwind CLARIFY (CLoud–Aerosol–Radiation Interaction and Forcing) campaign during the sampling time. The solid lines in **c, d** are the fitted size distributions for ORACLES, and dashed lines are fitted size distributions for CLARIFY. The Grey colour represents cases with no cloud processing, and the colourmap indicates the cloud liquid water content.

with the cloud layer. Although observational evidence of SOA aqueous formation is rare, our result is supported by numerous laboratory and modelling studies^{44,45}.

Variation of BB aerosol size distribution. From Fig. 3(a), the aerosol mode diameter D_m generally increases with ageing, consistent with previous findings²⁵. The increase of D_m can be up to 30 nm, exhibiting considerable changes in BB aerosol distribution by ageing. The geometric standard deviation σ also generally increases after further ageing for cases that show an apparent increase in D_m . Therefore, the variation in these two parameters indicates that aerosol size distribution broadens and shifts the peak towards larger diameters as it ages. Note that due to missing values in the observations, only one dry sample is available after prolonged ageing, implying that there may be large uncertainties in the results of dry samples. Nevertheless, cloud processing clearly increases D_m , and the increase in D_m is greater for samples with longer ageing hours and experiencing cloud processing with higher liquid water. However, for cases where the σ is clearly increased, strong cloud processing tends to reduce the $\Delta \sigma$ ($\Delta \sigma$ still >0 , Fig. 3b), suggesting that cloud processing can narrow the aerosol size distribution. To provide a clearer view of the evolution of aerosol size distribution with ageing, two examples with similar ageing in hours but different cloud processing (with and without) were selected for further illustration. The two samples selected are enclosed in the black boxes in Fig. 3(a, b), and the corresponding variations in the number size distribution with ageing are shown in Fig. 3(c, d).

Compared to the dry sample, the particle concentration of the wet sample decreases substantially after ageing, demonstrating the considerable effect of cloud processing in removing aerosols. For

both cases, ageing broadens particle size distributions and shifts them towards larger diameters (ΔD_m and $\Delta \sigma > 0$), resulting in a decrease in aerosols at the small sizes (<200 nm), and an increase in large particles (>200 nm) for the dry sample. The possible reason for the decrease in small-sized particles for the dry sample is coagulation, since the condensation growth would become very slow or even stops with sufficient ageing, while coagulation can still occur. The strong inversion under the plume layer may have prevented the vertical dilution of the plume, thus facilitating coagulation growth. Although coagulation should be much more obvious in fresher BB aerosols, this result highlights the importance of its role for very aged plumes in the SEA. For the wet sample, particles below 400 nm decrease with ageing and cloud processing, while above 400 nm, the changes are less pronounced. This may be due to the inherently low concentration of particles above 400 nm in diameter that may mix with cloud residuals, which have a large size, as they exit the clouds. For the dry sample, particles above 200 nm increase after ageing. This result is consistent with the findings of Capes et al.²⁵, who used a coagulation box model to simulate the changes in the particle size distribution with ageing for African BB aerosols, and found that coagulation mainly affects particles below 100 nm. Therefore, coagulation alone is unable to explain the observed increase in large particles, which may be more likely due to the entrainment of multiple plumes into the same air parcel and size-dependent condensation and re-evaporation processes. Compare these two cases; it can be seen that the aged aerosol distribution (from CLARIFY, CLoud–Aerosol–Radiation Interaction and Forcing campaign) is narrower in the case with cloud processing, as demonstrated by the lower fraction of larger particles (>200 nm). Therefore, the reduction of σ by cloud processing is mainly reflected in the removal of large particles. In general,

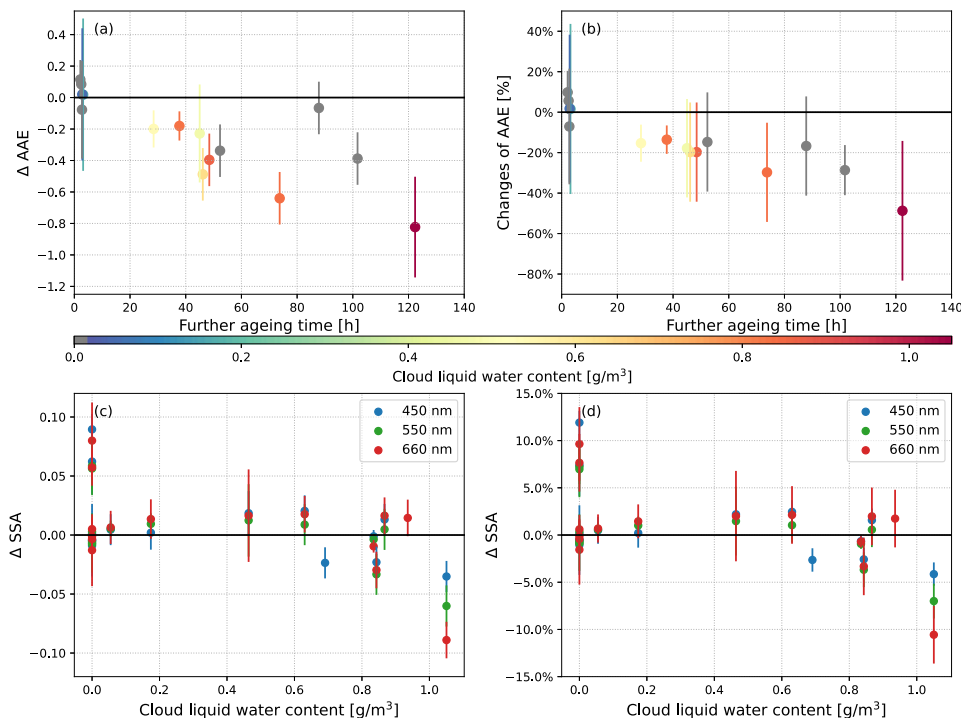


Fig. 4 Evolution of aerosol optical properties with ageing. **a** Absorption Ångström exponent (AAE) and **b** the corresponding changes of AAE in percentage with further ageing time; **c** the impact of cloud processing on single-scattering albedo (SSA); and **d** the corresponding changes of SSA in percentage. The dots are mean values, and the error bars are standard errors from Gaussian error propagation. The grey colour in **a**, **b** represents cases with no cloud processing, while the colour map represents the cloud liquid water content. Blue, green, and red dots in **c**, **d** represent SSA at different wavelengths.

ageing shifts the aerosol distribution towards larger sizes and increases the proportion of large particles. With the increase of the aerosol hygroscopicity resulting from f_{44} increasing, the ageing process can be an important source of CCN, especially in the intermediate and clean SEA marine boundary layer⁴⁶.

Variation of BB aerosol optical properties. The changes in AAE with ageing and cloud processing are illustrated in Fig. 4(a, b). Overall, AAE decreases with ageing. The longer it ages, the greater the decrease, with a maximum reduction of AAE up to 50%. The decrease of AAE indicates the diminishing of the wavelength dependence of the light-absorption coefficient of BB aerosol, which may be caused by the photochemical degradation of BrC and variations in the aerosols size distribution. In general, AAE is highly sensitive to particle size distribution for compact and coated BC, with large particles having a smaller AAE⁴⁷. As we have shown in the previous section, ageing increases the mode diameter of aerosol distribution, which may be responsible for the AAE reduction. Mie model simulations suggest the variations in the aerosol number size distribution may be the main reason for the decrease in AAE (Supplementary Fig. 8). However, changes in the size distribution can only account for a partial decrease in AAE (more than 50%), suggesting it is not sufficient to explain the observed reduction in AAE. Therefore, the reduction of BrC might also contribute to the decrease in AAE. As the absorption coefficient of BrC has a strong spectral dependence than that of BC, photobleaching of BrC leads to a decrease in AAE, which can be used along with the variation in aerosol size distribution to explain the reduction in AAE in dry samples. This finding is consistent with the result of aerosol optical closure studies in the region, which suggests upwind ORACLES (ObseRvations of Aerosols above CLouds and their intERactionS)⁴⁸ have more BrC than downwind CLARIFY⁴⁹ observations. For wet cases, the mode diameters of aerosol size distributions increase with ageing,

resulting in a decrease in AAE. In addition to that, the removal of BrC also contributed to the decrease in AAE in the wet samples. The aqueous-phase processing and oligomerisation of water-soluble organics have been recognised to form light-absorbing BrC, suggesting cloud processing is an important source of BrC⁵⁰. However, our results find AAE decreases even more for stronger cloud processing cases, suggesting that the contribution of BrC from the aqueous-phase reaction is overridden by wet removal. This is because BrC is generally considered to be hygroscopic³⁰, as even tarballs, the most refractive and least hygroscopic BrC, is able to completely dissolve in a water droplet under supersaturation⁵¹. Therefore, its hygroscopic properties lead to the dominance of the wet removal of BrC, resulting in a decrease in AAE.

The trend of Δ SSA with ageing is less clear due to the limited data (Supplementary Fig. 9). However, we find Δ SSA generally decreases with cloud liquid water content (Fig. 4c, d). For cases with cloud liquid water content smaller than 0.6 g/m^3 , Δ SSA is approximately equal to or greater than 0, suggesting the possible increase in SSA for aged BB aerosol. Haywood et al. studied fresh⁵² and 5 h aged⁵³ BB plumes in Southern Africa during SAFARI-2000 and also found that the aged BB aerosol has a higher SSA, likely due to the condensation of scattering material and change in black carbon (BC) morphology from a chain agglomerate to a more spheroidal shape⁵⁴. The BB plume in our study is more aged with mostly compact BC⁴¹. However, as we illustrated previously, ageing can increase the large particle fraction. Since scattering is highly dependent on diameters, such an increase can result in an increase in SSA. For samples with stronger cloud processing, SSA decreases. The higher the cloud processing intensity, the larger the reduction of SSA. The decrease of SSA due to cloud processing can be up to approximately 10%, and may result from the wet removal of large particles and thickly coated BC by cloud droplets. Mie model simulations confirm that variations in aerosol number size distribution are the main factor

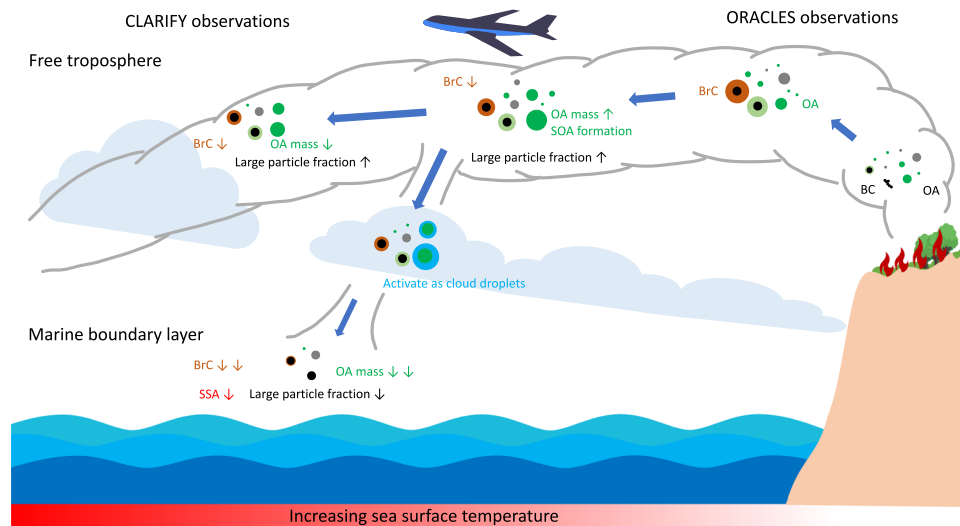


Fig. 5 Schematic showing the evolution of biomass burning aerosols with ageing and cloud processing during the westward transport in the south-eastern Atlantic. For a clear visualisation of the aerosol changes, most of the aerosols in the figure are externally mixed, which would not match reality, and the actual aerosol mixing is beyond the scope of this paper. During transport, changes in aerosols are illustrated by small upward and downward arrows, indicating increases and decreases. Two of such arrows suggest a significant change. Note those changes are compared to the previous step connected by the big blue arrow.

contributing to the decrease in SSA. Ground-based in-situ measurements on Ascension Island showed the lowest SSA values compared to all previously reported aircraft observations in the SEA^{39,55}, which can be explained by cloud processing, as the BB plume needs to travel through the extensive stratocumulus cloud deck to reach their sampling location.

Conclusions

By linking observations from upwind and downwind areas with trajectories, we investigated the BB aerosol evolution with ageing in the SEA. The main conclusions are illustrated schematically by Fig. 5. All BB aerosols measured are emitted from flaming fires, with MCE all above 0.98. Our results suggest SOA formation prevails when the further ageing time is less than ~30 h. Taking the average age of BB aerosols measured at the upwind location ~40 h into account (Supplementary Table 1), it may suggest SOA formation dominates at high CO concentrations for 70 h of transport of the BB plume after emission. This time scale is much longer than previous studies, partly because the strong inversion layer below the plume has prevented vertical diffusion, resulting in relatively high levels of volatile organic compounds in the plume. This finding of SOA formation after a long transport time has important implications on the regional climate, as SOA can modulate BB aerosol direct and semi-direct radiative forcings by affecting BBA optical properties. SOA can also affect the indirect radiative forcing by providing more CCN, as it has a higher hygroscopicity. After ~30 h of further ageing (~70 h in total), SOA formation rates may have dropped to a very low level, resulting in the decrease of OA mass, which may be related to the photolysis or OH induced fragmentation reactions. At ~60 h of further ageing (~100 h in total), OA mass falls back to the approximate amount measured in the upwind and generally remains constant afterwards, implying that OA is in a dynamic equilibrium between SOA formation and photolysis. However, it is still higher than that freshly emitted, considering the formation of SOA in the first 40 h after emission. These results can provide key information on the time scales of different effects on the long-lived BB aerosols in the SEA, contributing to better model parameterisation. Cloud processing shows a clear reduction in OA mass, showing a strong wet removal of OA; however, cloud processing is accompanied by an increase in temperature,

suggesting that it may have also led to the reduction in OA mass. The oxidised OA fraction f_{44} increases steadily with ageing, regardless of whether the aerosol has undergone cloud processing, and even more markedly if it has, suggesting the continuous oxidation of OA and highlighting aqueous-phase oxidation by clouds. Besides its effect on BB aerosol chemical composition, ageing can also change the physical properties of BB aerosols. With ageing, aerosol size distribution shifts towards larger diameters resulting in an increase in CCN, which is very important in the SEA, as the emitted BB aerosol would eventually subside and meet the gradually deepening marine boundary layer⁵⁶. Comparing aged aerosols that have experienced cloud processing with those not with a similar ageing time, cloud processing shows an effective removal effect for large particles.

As a result of physical and chemical changes of BB aerosol caused by ageing and cloud processing, its optical properties evolve correspondingly. The decrease of AAE may be driven by a combination of factors; the main factor is the increase in particle size with ageing, as larger particles have a lower AAE. However, variations in aerosol size distribution alone are not sufficient to explain the observed decrease in AAE, suggesting the photochemical bleaching of BrC with ageing may be another reason for the reduction of AAE. Sedlacek III et al. (from personal communication) find a decrease in BC coating after a long period of transport of BB plume, which could also be another reason for the decreases in AAE. For those aerosols that experience cloud processing, one additional reason for the decrease in AAE is the wet removal of BrC, which is generally hygroscopic and can completely dissolve in water droplets under supersaturation. We also find SSA decreases with cloud processing, which may happen because cloud processing removes large particles and makes BC more compact. In addition, thickly coated BC particles can also be removed by clouds, as they have a higher hygroscopicity. The reduction of SSA by clouds may suggest the BB aerosol in the SEA boundary layer is more absorbing, as BB aerosols generally need to travel through clouds to reach the marine boundary layer. Those changes in SSA may have a vital effect on the regional radiation balance, as the direct radiative forcing of BB aerosol is sensitive to the SSA⁹. However, as the number of linked samples is relatively scarce, we encourage more multiple aircraft observations to untangle the BB aerosol-cloud-radiation interactions caused by aerosol ageing.

Materials and methods

Aircraft measurements. Aircraft observation campaigns of ORACLES (Observations of Aerosols above CLouds and their intERactions) and CLARIFY (Cloud–Aerosol–Radiation Interaction and Forcing) were conducted in different areas over the SEA. The ORACLES aircraft campaign was based from São Tomé in 2017, and flew in the upwind area of the SEA⁵⁷, while CLARIFY was based from Ascension Island, and flew in the downwind regions¹⁵. The fire counts, aircraft tracks, mean aerosol optical depths, and mean low-cloud fraction during the flight observation can be seen in Supplementary Fig. 1. These two campaigns cover a large area with mean low-cloud fractions ranging from 0.7 to 0.4 and mean aerosol optical depths from 1.2 to 0.4, respectively. A brief description of the data we used is presented in this section, while a more detailed one can be found in campaign overviews^{15,57}. Black carbon (BC) mass concentration was measured by the Single Particle Soot Photometer (SP2), and non-refractory aerosol chemical composition was measured by Aerodyne C-ToF-aerosol mass spectrometer (AMS) in CLARIFY and HR-ToF-AMS in ORACLES. Carbon monoxide (CO) was measured by Los Gatos Research CO/CO₂/H₂O analyser in ORACLES and vacuum ultraviolet fluorescence spectroscopy (AL5002, Aerolaser GmbH) in CLARIFY. The aerosol scattering and absorption coefficients were measured by nephelometers and particle soot absorption photometer (PSAP) in ORACLES, while CLARIFY used the EXSCALABAR instrument (Extinction Scattering and Absorption of Light for Air-Borne Aerosol Research). The absorption, scattering, and extinction coefficients from both campaigns are converted to 450, 550, and 660 nm wavelength for comparison by calculating the Ångström exponent. For the aerosol size distribution, we use the ultra-high-sensitivity aerosol spectrometer (UHSAS) data for particles ranging from 60 to 1000 nm in ORACLES; while for CLARIFY, we use the Passive Cavity Aerosol Spectrometer Probe (PCASP) data for particles from 100 nm to 3 µm, and the Scanning Mobility Particle Size Spectrometer (SMPS) for particles below 100 nm. An undersized issue by UHSAS was detected, and a correction function was applied for ORACLES data⁵⁸. During the campaigns, an intercomparison between ORACLES and CLARIFY aircraft observation was conducted on 18 August 2017 to ensure measurements from different aircraft were comparable⁵⁹. Although the aerosol concentration was very low during the intercomparison flights, the CO observations showed fairly good agreement. A detailed comparison can be found in Supplementary Note 1. All variables have been converted under the standard temperature and pressure (STP) for the ensuing analysis.

Trajectory linking. We use air mass trajectories calculated by the Hybrid Single-Particle Lagrangian Integrated Trajectory model (HYSPPLIT)⁶⁰ to link ORACLES and CLARIFY observations. To improve the accuracy, we use hourly high resolution (0.25° × 0.25°) ERA5 reanalysis (fifth generation of ECMWF reanalysis data) for the calculation. There are five main procedures to ensure the success of the linking. (1) Identify and limit analysis to only straight-level runs from ORACLES flights. (2) Launch forward trajectory at the coordinate of straight-level runs of each ORACLES aircraft, calculate a trajectory per minute, with a time step of the trajectory of 20 min. (3) Calculate the horizontal and vertical distance between the air mass and aircraft of CLARIFY and other ORACLES flight at each time step. If the horizontal distance is within 0.5° and the vertical distance is within 500 m, then the case is identified as potentially linked. (4) In those potentially linked cases, if the total sampling time is over 2 min, and there is no obvious change between the linked trajectory and other trajectories launched at the adjacent times from the upwind ORACLES, then the air mass is marked as “successfully linked”. (5) For those linked air masses, estimate the initial age of the BB aerosols measured from upwind ORACLES aircraft (detailed in Supplementary Note 2). Only select those with an ageing time of fewer than 48 h (remove already very aged samples) and remove cases with data below the detection limit for further analysis. The successfully linked cases are illustrated in Supplementary Fig. 4, along with their air mass trajectories. In total, 23 linked cases have been identified, with 11 ORACLES linked with CLARIFY cases and 12 ORACLES cases linked with ORACLES itself (Table S1). The linking procedure allows the investigation of samples measured in the exact same air mass but at different times, where the evolution of aerosols can be analysed by the Lagrangian methodology.

Satellite data. The Spinning Enhanced Visible and InfraRed Imager (SEVIRI) on the Meteosat Second Generation satellite was utilized here, using cloud properties generated by NASA Langley⁶¹. The SEVIRI cloud data has a high resolution (3 km at the subsatellite point with a repeat cycle of 15 min) and was used to provide cloud processing information by collocating with the linked trajectories. An air mass that experiences cloud processing was defined as one with cloud liquid water content above 0.01 g m⁻³ on its trajectory, and an air mass height above cloud base and below cloud top. The accumulated cloud liquid water content within 24 h before the air mass reached the downwind linked location was calculated and used in our analysis. By considering the aerosol cloud processing in the last day of transport, we assume that aerosols are not subject to mixing and other ageing effects in the 24 h after being in-cloud. As the cloud processing estimate requires the vertical height of the cloud, the uncertainty in SEVIRI cloud height can therefore lead to uncertainties in the cloud processing⁶². Supplementary Fig. 5 shows an example of a linked case with cloud processing along with its trajectory.

The GPM (Global Precipitation Measurement) IMERG (Integrated Multi-satellite Retrievals for GPM) precipitation V06 final run data⁶³ was used to identify

precipitation. The data has a high spatial resolution of 0.1 degrees and is available every half hour. During the transport of the air mass, if the height of the trajectory was lower than the height of the cloud base, and precipitation was present at the location of the air mass, the air mass was determined to be influenced by precipitation. Only one sample showed a slight influence due to precipitation, with an accumulated precipitation of around 0.003 mm. We removed this sample to remove the effects of precipitation from our linked cases.

Linked measurement analysis. To determine the evolution of OA mass, we calculated the OA enhancement factor $\Delta(OA/CO)$ as in Eq. (1) to examine the change of OA mass by removing the dilution effect.

$$\Delta \frac{OA}{CO} = \frac{OA_{down}}{CO_{down}} - \frac{OA_{up}}{CO_{up}} \quad (1)$$

The subscripts “down” and “up” indicate downwind and upwind observations, respectively. CO is used as a conservative tracer to account for dilution, as it has a lifetime of approximately a month. The units of CO have been transformed into the same weight unit of OA; thus, the OA/CO is unitless. Positive values of $\Delta(OA/CO)$ indicate an increase in OA mass along with the air mass transport, implying the formation of SOA. A zero value of $\Delta(OA/CO)$ means there is no net change of OA mass along with the transportation, while negative values indicate a decrease in OA mass. Next, we calculated OA mass concentration downwind (OA_{down}^{calc}) by assuming only dilution is affecting the OA mass, as in Eq. (2). Therefore, changes in OA mass with ageing can be calculated in percentage, as in Eq. (3).

$$OA_{down}^{calc} = \frac{OA_{up}}{CO_{up}} * CO_{down} \quad (2)$$

$$f_{OA} = \frac{OA_{down} - OA_{down}^{calc}}{OA_{down}^{calc}} * 100\% \quad (3)$$

The OA oxidation level is represented by f_{44} calculated from AMS data. The difference of f_{44} between the upwind and downwind observations is calculated as in Eq. (4), and the change in f_{44} in percentage can be calculated as in Eq. (5)

$$\Delta f_{44} = f_{44,down} - f_{44,up} \quad (4)$$

$$f_{f_{44}} = \frac{\Delta f_{44}}{f_{44,up}} * 100\% \quad (5)$$

The AAE at upwind and downwind locations of air mass trajectories are calculated between 450 and 660 nm wavelengths as in Eq. (6). Then the differences are calculated as in Eq. (7) to study the changes of AAE with ageing.

$$AAE = - \frac{\ln(\sigma_{450}/\sigma_{660})}{\ln(450/660)} \quad (6)$$

$$\Delta AAE = AAE_{down} - AAE_{up} \quad (7)$$

where the σ_{450} and σ_{660} denote the aerosol absorption coefficient at 450 and 660 nm, respectively. SSA is calculated in Eq. (8), and the change of SSA by Eq. (9).

$$SSA = \sigma_{scattering} / \sigma_{extinction} \quad (8)$$

$$\Delta SSA = SSA_{down} - SSA_{up} \quad (9)$$

where $\sigma_{extinction}$ and $\sigma_{scattering}$ are extinction and scattering coefficients of BB aerosol. The changes in AAE and SSA in percentage can be calculated in Eqs. (10–11).

$$f_{AAE} = \frac{\Delta AAE}{AAE_{up}} * 100\% \quad (10)$$

$$f_{SSA} = \frac{\Delta SSA}{SSA_{up}} * 100\% \quad (11)$$

Uncertainties of the parameters in each linked case are estimated by the Gaussian error propagation with the measured data. Note that only the uncertainty of the data during the observation is considered; the error of the instrument is not included in the calculation.

Data availability

Data from the CLARIFY aircraft campaign are available on the CEDA repository at <http://catalogue.ceda.ac.uk/uuid/38ab7089781a4560b067dd6c20af3769> (last access: 2022-07-04). Data from ORACLES aircraft campaigns are available on the repository at <https://espo.nasa.gov/oracles/archive/browse/oracles/id14> (last access: 2022-07-04). ERA5 reanalysis data (<https://doi.org/10.24381/cds.bd0915c6>) can be obtained from <https://cds.climate.copernicus.eu>. The SEVIRI cloud product are provided by NASA Langley, and are available in: <https://satcorps.larc.nasa.gov/cgi-bin/site/showdoc?docid=22&tkdomain=Y&domain=ORACLES> (last access: 2022-07-04). GPM precipitation data (<https://doi.org/10.5067/GPM/IMERG/3B-HH/06>) can be obtained from: <https://disc>.

gfs.nasa.gov/datasets/GPM_3IMERGHH_06/summary (last access: 2022-07-04). SEVIRI fire data in Supplements are from the geostationary satellite Meteosat-8, and can be obtained from: <https://navigator.eumetsat.int/product/EO:EUM:DAT:MSG:FRP-SEVIRI> (last access: 2022-07-04). MODIS wildfire data (<https://doi.org/10.5067/FIRMS/MODIS/MCD14DL.NRT.0061>) in supplements are from NASA FIRMS <https://earthdata.nasa.gov/firms> (last access: 2022-07-04).

Received: 3 September 2021; Accepted: 3 August 2022;

Published online: 18 August 2022

References

- Roberts, G., Wooster, M. J. & Lagoudakis, E. Annual and diurnal African biomass burning temporal dynamics. *Biogeosciences* **6**, 849–866 (2009).
- van der Werf, G. R. et al. Global fire emissions estimates during 1997–2016. *Earth Syst. Sci. Data* **9**, 697–720 (2017).
- Che, H. et al. Seasonal variations in fire conditions are important drivers in the trend of aerosol optical properties over the south-eastern Atlantic. *Atmos. Chem. Phys.* **22**, 8767–8785 (2022).
- Che, H., Stier, P., Gordon, H., Watson-Parris, D. & Deaconu, L. Cloud adjustments dominate the overall negative aerosol radiative effects of biomass burning aerosols in UKESM1 climate model simulations over the south-eastern Atlantic. *Atmos. Chem. Phys.* **21**, 17–33 (2021).
- Sakaeda, N., Wood, R. & Rasch, P. J. Direct and semidirect aerosol effects of southern African biomass burning aerosol. *J. Geophys. Res.: Atmos.* **116**, D12205 (2011).
- Stier, P. et al. Host model uncertainties in aerosol forcing estimates: results from the AeroCom Prescribed intercomparison study. *Atmos. Chem. Phys.* **13**, 3245–3270 (2013).
- Wilcox, E. M. Direct and semi-direct radiative forcing of smoke aerosols over clouds. *Atmos. Chem. Phys.* **12**, 139–149 (2012).
- de Graaf, M. et al. Comparison of south-east Atlantic aerosol direct radiative effect over clouds from SCIAMACHY, POLDER and OMI–MODIS. *Atmos. Chem. Phys.* **20**, 6707–6723 (2020).
- Mallet, M. et al. Direct and semi-direct radiative forcing of biomass-burning aerosols over the southeast Atlantic (SEA) and its sensitivity to absorbing properties: a regional climate modeling study. *Atmos. Chem. Phys.* **20**, 13191–13216 (2020).
- Akagi, S. K. et al. Evolution of trace gases and particles emitted by a chaparral fire in California. *Atmos. Chem. Phys.* **12**, 1397–1421 (2012).
- Denjean, C. et al. Unexpected Biomass burning aerosol absorption enhancement explained by black carbon mixing state. *Geophys. Res. Lett.* **47**, e2020GL089055 (2020).
- Hodshire, A. L. et al. Aging effects on biomass burning aerosol mass and composition: a critical review of field and laboratory studies. *Environ. Sci. Technol.* **53**, 10007–10022 (2019).
- Adachi, K. et al. Spherical tarball particles form through rapid chemical and physical changes of organic matter in biomass-burning smoke. *Proc. Natl Acad. Sci.* **116**, 19336–19341 (2019).
- Zhang, Q. et al. Understanding composition, formation, and aging of organic aerosols in wildfire emissions via combined mountain top and airborne measurements. in *Multiphase Environmental Chemistry in the Atmosphere* vol. 1299 363–385 (American Chemical Society, 2018).
- Haywood, J. M. et al. The CLOUD–Aerosol–Radiation Interaction and Forcing: Year 2017 (CLARIFY-2017) measurement campaign. *Atmos. Chem. Phys.* **21**, 1049–1084 (2021).
- Wu, H. et al. Vertical variability of the properties of highly aged biomass burning aerosol transported over the southeast Atlantic during CLARIFY-2017. *Atmos. Chem. Phys.* **20**, 12697–12719 (2020).
- Bian, Q. et al. Secondary organic aerosol formation in biomass-burning plumes: theoretical analysis of lab studies and ambient plumes. *Atmos. Chem. Phys.* **17**, 5459–5475 (2017).
- Chacon-Madrid, H. J. & Donahue, N. M. Fragmentation vs. functionalization: chemical aging and organic aerosol formation. *Atmos. Chem. Phys.* **11**, 10553–10563 (2011).
- Lim, C. Y. et al. Secondary organic aerosol formation from the laboratory oxidation of biomass burning emissions. *Atmos. Chem. Phys.* **19**, 12797–12809 (2019).
- Ortega, A. M. et al. Secondary organic aerosol formation and primary organic aerosol oxidation from biomass-burning smoke in a flow reactor during FLAME-3. *Atmos. Chem. Phys.* **13**, 11551–11571 (2013).
- Tkacik, D. S. et al. A dual-chamber method for quantifying the effects of atmospheric perturbations on secondary organic aerosol formation from biomass burning emissions. *J. Geophys. Res.: Atmos.* **122**, 6043–6058 (2017).
- DeCarlo, P. F. et al. Fast airborne aerosol size and chemistry measurements above Mexico City and Central Mexico during the MILAGRO campaign. *Atmos. Chem. Phys.* **8**, 4027–4048 (2008).
- Vakkari, V. et al. Major secondary aerosol formation in southern African open biomass burning plumes. *Nat. Geosci.* **11**, 580–583 (2018).
- Yokelson, R. J. et al. Emissions from biomass burning in the Yucatan. *Atmos. Chem. Phys.* **9**, 5785–5812 (2009).
- Capes, G. et al. Aging of biomass burning aerosols over West Africa: Aircraft measurements of chemical composition, microphysical properties, and emission ratios. *J. Geophys. Res.: Atmos.* **113**, D00C15 (2008).
- Forrister, H. et al. Evolution of brown carbon in wildfire plumes. *Geophys. Res. Lett.* **42**, 4623–4630 (2015).
- Hecobian, A. et al. Comparison of chemical characteristics of 495 biomass burning plumes intercepted by the NASA DC-8 aircraft during the ARCTAS/CARB-2008 field campaign. *Atmos. Chem. Phys.* **11**, 13325–13337 (2011).
- May, A. A. et al. Observations and analysis of organic aerosol evolution in some prescribed fire smoke plumes. *Atmos. Chem. Phys.* **15**, 6323–6335 (2015).
- Morgan, W. T. et al. Transformation and ageing of biomass burning carbonaceous aerosol over tropical South America from aircraft in situ measurements during SAMBBA. *Atmos. Chem. Phys.* **20**, 5309–5326 (2020).
- Laskin, A., Laskin, J. & Nizkorodov, S. A. Chemistry of atmospheric brown carbon. *Chem. Rev.* **115**, 4335–4382 (2015).
- Nguyen, T. B. et al. Formation of nitrogen- and sulfur-containing light-absorbing compounds accelerated by evaporation of water from secondary organic aerosols. *J. Geophys. Res.: Atmos.* **117**, D01207 (2012).
- Lee, A. K. Y. et al. Formation of light absorbing organo-nitrogen species from evaporation of droplets containing glyoxal and ammonium sulfate. *Environ. Sci. Technol.* **47**, 12819–12826 (2013).
- Powelson, M. H., Espelien, B. M., Hawkins, L. N., Galloway, M. M. & De Haan, D. O. Brown carbon formation by aqueous-phase carbonyl compound reactions with amines and ammonium sulfate. *Environ. Sci. Technol.* **48**, 985–993 (2014).
- Marrero-Ortiz, W. et al. Formation and optical properties of brown carbon from small α -dicarbonyls and amines. *Environ. Sci. Technol.* **53**, 117–126 (2019).
- Konovalov, I. B., Golovushkin, N. A., Beekmann, M. & Andreae, M. O. Insights into the aging of biomass burning aerosol from satellite observations and 3D atmospheric modeling: evolution of the aerosol optical properties in Siberian wildfire plumes. *Atmos. Chem. Phys.* **21**, 357–392 (2021).
- Bond, T. C., Zarzycki, C., Flanner, M. G. & Koch, D. M. Quantifying immediate radiative forcing by black carbon and organic matter with the Specific Forcing Pulse. *Atmos. Chem. Phys.* **11**, 1505–1525 (2011).
- Doherty, S. J. et al. Modeled and observed properties related to the direct aerosol radiative effect of biomass burning aerosol over the southeastern Atlantic. *Atmos. Chem. Phys.* **22**, 1–46 (2022).
- Bianco, A., Passananti, M., Brigante, M. & Mailhot, G. Photochemistry of the Cloud Aqueous Phase: A review. *Molecules* **25**, 423 (2020).
- Zuidema, P. et al. The ascension island boundary layer in the remote southeast Atlantic is often smoky. *Geophys. Res. Lett.* **45**, 4456–4465 (2018).
- Flossmann, A. I. & Wobrock, W. Cloud processing of aerosol particles in marine stratocumulus clouds. *Atmosphere* **10**, 520 (2019).
- Dang, C. et al. Biomass burning and marine aerosol processing over the southeast Atlantic Ocean: a TEM single-particle analysis. *Atmos. Chem. Phys.* **22**, 9389–9412 (2022).
- Aiken, A. C. et al. O/C and OM/OC ratios of primary, secondary, and ambient organic aerosols with high-resolution Time-of-Flight Aerosol Mass Spectrometry. *Environ. Sci. Technol.* **42**, 4478–4485 (2008).
- Frosch, M. et al. Relating cloud condensation nuclei activity and oxidation level of α -pinene secondary organic aerosols. *J. Geophys. Res.: Atmos.* **116**, D22212 (2011).
- Ervens, B., Turpin, B. J. & Weber, R. J. Secondary organic aerosol formation in cloud droplets and aqueous particles (aqSOA): a review of laboratory, field and model studies. *Atmos. Chem. Phys.* **11**, 11069–11102 (2011).
- Lim, Y. B., Tan, Y., Perri, M. J., Seitzinger, S. P. & Turpin, B. J. Aqueous chemistry and its role in secondary organic aerosol (SOA) formation. *Atmos. Chem. Phys.* **10**, 10521–10539 (2010).
- Kacarab, M. et al. Biomass burning aerosol as a modulator of the droplet number in the southeast Atlantic region. *Atmos. Chem. Phys.* **20**, 3029–3040 (2020).
- Liu, C., Chung, C. E., Yin, Y. & Schnaiter, M. The absorption Ångström exponent of black carbon: from numerical aspects. *Atmos. Chem. Phys.* **18**, 6259–6273 (2018).
- Zhang, L. et al. Light absorption by brown carbon over the South-East Atlantic Ocean. *Atmos. Chem. Phys.* **22**, 9199–9213 (2022).
- Taylor, J. W. et al. Absorption closure in highly aged biomass burning smoke. *Atmos. Chem. Phys.* **20**, 11201–11221 (2020).
- Graber, E. R. & Rudich, Y. Atmospheric HULIS: How humic-like are they? A comprehensive and critical review. *Atmos. Chem. Phys.* **6**, 729–753 (2006).
- Hand, J. L. et al. Optical, physical, and chemical properties of tar balls observed during the Yosemite Aerosol Characterization Study. *J. Geophys. Res.: Atmos.* **110**, D21210 (2005).

52. Haywood, J. M. et al. The mean physical and optical properties of regional haze dominated by biomass burning aerosol measured from the C-130 aircraft during SAFARI 2000. *J. Geophys. Res.: Atmos.* **108**, 8473 (2003).
53. Haywood, J., Francis, P., Dubovik, O., Glew, M. & Holben, B. Comparison of aerosol size distributions, radiative properties, and optical depths determined by aircraft observations and Sun photometers during SAFARI 2000. *J. Geophys. Res.: Atmos.* **108**, 8471 (2003).
54. Abel, S. J., Haywood, J. M., Highwood, E. J., Li, J. & Buseck, P. R. Evolution of biomass burning aerosol properties from an agricultural fire in southern Africa. *Geophys. Res. Lett.* **30**, 1783 (2003).
55. Pistone, K. et al. Intercomparison of biomass burning aerosol optical properties from in situ and remote-sensing instruments in ORACLES-2016. *Atmos. Chem. Phys.* **19**, 9181–9208 (2019).
56. Adebisi, A. A., Zuidema, P. & Abel, S. J. The convolution of dynamics and moisture with the presence of shortwave absorbing aerosols over the southeast Atlantic. *J. Clim.* **28**, 1997–2024 (2015).
57. Redemann, J. et al. An overview of the ORACLES (ObseRvations of Aerosols above CLouds and their intERactions) project: aerosol–cloud–radiation interactions in the southeast Atlantic basin. *Atmos. Chem. Phys.* **21**, 1507–1563 (2021).
58. Howell, S. G., Freitag, S., Dobracki, A., Smirnov, N. & Sedlacek III, A. J. Undersizing of aged African biomass burning aerosol by an ultra high sensitivity aerosol spectrometer. *Atmos. Meas. Tech. Discuss.* 1–28 <https://doi.org/10.5194/amt-2020-416> (2020).
59. Barrett, P. A. et al. Intercomparison of airborne and surface-based measurements during the CLARIFY, ORACLES and LASIC field experiments. *Atmos. Meas. Tech. Discuss.* 1–60 <https://doi.org/10.5194/amt-2022-59> (2022).
60. Stein, A. F. et al. NOAA’s HYSPLIT atmospheric transport and dispersion modeling system. *Bull. Am. Meteorol. Soc.* **96**, 2059–2077 (2015).
61. Minnis, P. et al. CERES Edition-2 cloud property retrievals using TRMM VIRS and Terra and Aqua MODIS Data—Part I: Algorithms. *IEEE Trans. Geosci. Remote Sens.* **49**, 4374–4400 (2011).
62. Hamann, U. et al. Remote sensing of cloud top pressure/height from SEVIRI: analysis of ten current retrieval algorithms. *Atmos. Meas. Tech.* **7**, 2839–2867 (2014).
63. Huffman, G. J., Stocker, E. F., Bolvin, D. T., Nelkin, E. J. & Tan, J. GPM IMERG Final Precipitation L3 1 day 0.1 degree x 0.1 degree V06, Edited by Andrey Savtchenko, Greenbelt, MD, Goddard Earth Sciences Data and Information Services Center (GES DISC). <https://doi.org/10.5067/GPM/IMERGDF/DAY/06> (2019).

Acknowledgements

The authors would like to thank the ORACLES team, CLARIFY team and the funding of the project by the DOE-ASR grant DE-SC0020084. This work benefitted from support from the CLARIFY NERC Large Grant NE/L013584/1, and support from ORACLES

NASA through the Earth Venture Suborbital-2 (EVS-2) program Grant 13-EVS2-13-0028.

Author contributions

H.C.C. and M.S.R. conceived the idea and led the study. P.Z., A.D., A.J.S., H.C., H.W., J.T., J.R., and J.H. provided data. L.Z. and C.D. contributed data analysis. H.C.C. wrote the manuscript with comments from all co-authors. M.S.R., L.Z., C.D., P.Z., A.J.S., J.T., X.Z., and J.R. reviewed and revised the manuscript. M.S.R., L.Z., and C.D. helped with the proofreading.

Competing interests

The authors declare no competing interests.

Additional information

Supplementary information The online version contains supplementary material available at <https://doi.org/10.1038/s43247-022-00517-3>.

Correspondence and requests for materials should be addressed to Haochi Che or Michal Segal-Rozenhaimer.

Peer review information *Communications Earth & Environment* thanks Matthias Beekmann and the other, anonymous, reviewer(s) for their contribution to the peer review of this work. Primary Handling Editors: Kerstin Schepanski, Joe Aslin and Clare Davis. Peer reviewer reports are available.

Reprints and permission information is available at <http://www.nature.com/reprints>

Publisher’s note Springer Nature remains neutral with regard to jurisdictional claims in published maps and institutional affiliations.



Open Access This article is licensed under a Creative Commons

Attribution 4.0 International License, which permits use, sharing, adaptation, distribution and reproduction in any medium or format, as long as you give appropriate credit to the original author(s) and the source, provide a link to the Creative Commons license, and indicate if changes were made. The images or other third party material in this article are included in the article’s Creative Commons license, unless indicated otherwise in a credit line to the material. If material is not included in the article’s Creative Commons license and your intended use is not permitted by statutory regulation or exceeds the permitted use, you will need to obtain permission directly from the copyright holder. To view a copy of this license, visit <http://creativecommons.org/licenses/by/4.0/>.

© The Author(s) 2022